# **Accepted Manuscript**

Phase relationships in the CeFe<sub>8</sub>Co<sub>3</sub>Ti<sub>1-v</sub>Si<sub>v</sub> system

B.S. Conner, M.A. McGuire, M.A. Susner, B.C. Sales

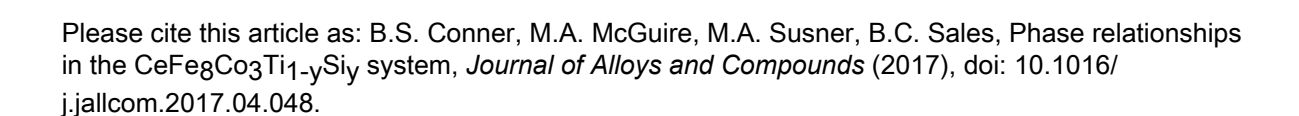
PII: S0925-8388(17)31224-0

DOI: 10.1016/j.jallcom.2017.04.048

Reference: JALCOM 41449

To appear in: Journal of Alloys and Compounds

Received Date: 3 January 2017
Revised Date: 25 March 2017
Accepted Date: 4 April 2017



This is a PDF file of an unedited manuscript that has been accepted for publication. As a service to our customers we are providing this early version of the manuscript. The manuscript will undergo copyediting, typesetting, and review of the resulting proof before it is published in its final form. Please note that during the production process errors may be discovered which could affect the content, and all legal disclaimers that apply to the journal pertain.



## Phase Relationships in the CeFe<sub>8</sub>Co<sub>3</sub>Ti<sub>1-v</sub>Si<sub>v</sub> System

B. S. Conner<sup>a</sup>, M. A. McGuire<sup>a</sup>, M. A. Susner <sup>\(\phi\)</sup>a, B. C. Sales<sup>a</sup>

<sup>a</sup>Materials Science and Technology Division, Oak Ridge National Laboratory, Oak Ridge, Tennessee 37831 USA

## Abstract

The phase formation behavior of the nominal CeFe<sub>8</sub>Co<sub>3</sub>Ti<sub>1-y</sub>Si<sub>y</sub> system is investigated for  $0 \le y \le 0.6$  by powder x-ray diffraction and scanning electron microscopy with energy dispersive x-ray spectroscopy for ingots formed by arc-melting then annealing at 1000 °C and quenching to room temperature. The ingots are seen to nearly single phase for  $y \le 0.4$  and are multi-phase for  $y \ge 0.5$  though a compound of the ThMn<sub>12</sub> type does indeed form for all values of y. The saturation magnetizations  $(M_s)$ , Curie temperatures  $(T_C)$ , and magnetic anisotropy fields  $(H_a)$  are measured for the  $y \le 0.4$  samples and the values of  $M_s$  and  $H_a$  appear to be nearly identical for all  $y \le 0.4$ .  $T_C$ , however, is seen to increase about 20 °C in this range for increasing y.

Keywords:

Permanent Magnet, Magnetic Anisotropy, Critical Materials,  $ThMn_{12}$ ,  $CeFe_{11}Ti$ ,  $CeFe_{11}Si$ ,  $TbCu_7$ ,  $Th_2Mn_7$ ,  $CaCu_5$ 

#### 1. Introduction

Iron-rich permanent magnets are ideal material systems for practical use due to abundance, cost, and performance considerations. To generate uniaxial magnetic anisotropy in iron rich compounds workers have previously investigated iron-rich phases that also include small percentages of rare-earth (RE) elements. The 4f electrons in these atoms generate large spin-orbit effects and contribute maximally to anisotropy. A result of these kinds of investigations was discovery of the compound  $\mathrm{Nd}_2\mathrm{Fe}_{14}\mathrm{B}$  and its doped analogs, which

Preprint submitted to Journal of Alloys and Compounds

have been exhaustively studied; see [1] for a review. The Nd<sub>2</sub>Fe<sub>14</sub>B family is perhaps the best magnet system ever discovered, boasting the largest room temperature energy products ever observed. However, the lackluster performance of Nd<sub>2</sub>Fe<sub>14</sub>B at elevated temperatures has led to studies of different structures with similar guiding principles in mind, that is to utilize RE elements in Fe rich compounds to achieve uniaxial anisotropy. Of course, Fe is cheap and the goal is always to maximize Fe:Re ratios while still maintaining acceptable uniaxial anisotropy and Curie temperatures,  $T_C$ . Research along these lines led to the discovery of permanent magnets having the  $ThMn_{12}$  structure type.  $ThMn_{12}$  is a tetragonal compound (space group I4/mmm) [2] which allows for the possibility of uniaxial magnetic anisotropy and one might expect excellent properties of the compound NdFe<sub>12</sub>, in analogy with the aforementioned Nd<sub>2</sub>Fe<sub>14</sub>B. Unfortunately, the NdFe<sub>12</sub> compound is unstable. However, early work on partial substitution on the iron sites for other elements, namely, V, Ti, Cr, Mn, Mo, W, Al, and Si, showed the possibility of structure stabilization [3, 4, 5, 6] for various species of RE atom in the Th site. Results from these studies on  $T_C$ and anisotropy field,  $H_a$ , were mixed, with some promising results depending on species. The suc-

 $<sup>^{\</sup>scriptsize \circ}$  Current Address of M. A. Susner is UES Inc., Beavercreek, OH 45432 USA

Email address: connerbs@ornl.gov (B. S. Conner)

This manuscript has been authored by UT-Battelle, LLC under Contract No. DE-AC05-00OR22725 with the U.S. Department of Energy. The United States Government retains and the publisher, by accepting the article for publication, acknowledges that the United States Government retains a non-exclusive, paid-up, irrevocable, worldwide license to publish or reproduce the published form of this manuscript, or allow others to do so, for United States Government purposes. The Department of Energy will provide public access to these results of federally sponsored research in accordance with the DOE Public Access Plan (http://energy.gov/downloads/doe-public-access-plan).

cess of these early works is the general motivation for the study of permanent magnets that take on this structure type.

Recent issues concerning rare-earth mining economics have forced researchers to focus their efforts on development of materials that utilize the elements lanthanum and cerium since the underuse of these resources is creating a great strain on that industry and negatively effecting the supply chain for more critical RE elements. See reference [7] for a pertinent example involving cerium utilization. The aforementioned promise of useable magnets with the  $ThMn_{12}$  structure and consideration of these economic issues has undoubtedly motivated the work described in two important papers whose observations we extend in our work here. In the first of these papers, Zhou et al. find that the compound CeFe<sub>11</sub>Ti is at least metastable and forms in the  $ThMn_{12}$  structure [8]. This finding confirms the earlier work of Pan et al. [9] and Akayama et al. [10]. Zhou et al. then investigate the saturation magnetization,  $M_s$ ,  $T_C$  and  $H_a$  of their melt-spun ribbon samples as they substitute cobalt into the iron site for the compound CeFe<sub>11-x</sub>Co<sub>x</sub>Ti. They find the maximum value for  $M_s$  of 125.0 emu/g at x = 3.  $T_C$  continually increases in the series for increasing x (T\_C= 467 °C for x = 3) and  $H_a$  decreases from  $H_a$ = 17.0 kOe at x = 0 to  $H_a$ =11.7 kOe at x = 3. In the second of the papers that directly motivate our work, Zhou et al. claim that the compound CeFe<sub>11</sub>Si also forms in the melt spinning process [11]. They claim that this compound has  $T_C=252$  °C and  $H_a=15.5$  kOe. In [8]  $T_C$  of CeFe<sub>11</sub>Ti is shown to be 209°C, making total Si substitution for Ti a positive move for  $T_C$  improvement if these results are correct.  $H_a$  is seen to degrade slightly, however, going from 17.0 kOe for the CeFe<sub>11</sub>Ti compound to 15.5 kOe for the CeFe<sub>11</sub>Si compound. In our work here we concentrate on the compound of maximum saturation magnetization, CeFe<sub>8</sub>Co<sub>3</sub>Ti, in [8] and ask what happens to the phase stability and magnetic properties as we substitute Si for Ti. We will label (and henceforth redefine x) this compound  $CeFe_8Co_3Ti_{1-x}Si_x$ . Note here that we do not imply that Si substitutes for Ti on the same atomic site; we can not determine their site preferences with the data presented here. We concern ourselves with the substitution by nominal composition as the only restriction and investigate said phase stability and magnetic properties.

## 2. Experimental

Ingots nominal composition CeFe<sub>8</sub>Co<sub>3</sub>Ti<sub>1-v</sub>Si<sub>v</sub> were created by arc-melting elemental Ce, Fe, Co, Ti, and Si. The ingots were then annealed in sealed quartz ampoules at 1000 °C for 150 hours and then rapidly quenched in water. Structural and phase characterization of the samples was performed via powder x-ray diffraction (PXRD), scanning electron microscopy (SEM) and electron dispersive x-ray (EDX) analysis. Powder x-ray diffraction experiments were performed on ground ingot samples. The instrument used for PXRD was a PANalytical XPert Pro diffractometer (Cu  $K_{\alpha 1}$ , 1.5406 Å). Refinements of the multi-phase ground-ingot samples were done with the FullProf software package [12]. SEM and EDX were performed on ingots that were polished then subjected to compositional analysis using a Hitachi TM-3000 electron microscope equipped with a Bruker Quantax 70 energy dispersive spectroscopy X-ray system. The saturation magnetization was measured for all samples at 300 K using a Quantum Design MPMS in applied external fields,  $H_{ext}$ , up to 60 kOe. Powders of each ingot for  $0 \le y \le 0.6$ were used to make field aligned samples as described previously [15] for hard axis field sweeps. The Curie temperatures,  $T_C$ , were obtained through thermal analysis using a Perkin Elmer Pyris Diamond Thermo-Gravimetric Analyzer/ Differential Thermal Analyzer (TGA/DTA).

## 3. Results and Discussion

## 3.1. Phase Analysis

The name  $CeFe_8Co_3Ti_{1-y}Si_y$  will be used to describe the nominal, desired composition of the  $CeFe_8Co_3Ti_{1-v}Si_v$  is, then, the final sample. overall composition used for the arc-melted ingots. This naming scheme can be contrasted with CeFe<sub>8</sub>Co<sub>3</sub>Ti<sub>1-x</sub>Si<sub>x</sub>, which represents the measured composition (by EDX) of the compound within the ingots with the ThMn<sub>12</sub> structure. In all cases reported in this work x = y with the exception of the y = 0.6 case. y=0.6 corresponds to a value of x = 0.55. Back-scatter SEM images of polished ingot surfaces are displayed in fig. 1(a)-(e). In all images small cerium oxide spots are observable and are the brightest features since the backscatter mode is sensitive to cerium content. Cerium oxide makes up only a tiny portion of the bulk and will be ignored in all analysis. In all images the

darkest regions are a solid solution that has the same structure as  $\alpha$  Fe and is made up predominantly of Fe and Co. For convenience we refer to these  $\alpha$  Fe type regions in this document with the symbol  $\Delta$ . Going from dark to light in fig. 1(a)-(e), we next observe the regions we shall refer to as  $\Phi$  regions. We believe the  $\Phi$  regions consist of one single-phase compound of the  $ThMn_{12}$  type. The  $\Phi$  regions are the main regions of interest here. The y=0, y=0.2, and y=0.4 back-scatter images of fig. 1 are completely dominated by  $\Phi$  regions. Another type of region, a  $\Omega$  region, is also observed but only in the y=0.5 and y=0.6 images. These regions appear brighter than the  $\Phi$  regions in fig. 1(a)-(e) and form predominantly around the  $\Delta$  regions in fig. 1(d) but are so prevalent in fig. 1(e) that they permeate the space of the entire sample. Because the contrast between  $\Phi$  and  $\Omega$  is difficult to distinguish in fig. 1(d)-(e), we show a false color Ti EDX map in fig. 1(f) to demonstrate the distinctness of the regions. We believe that the  $\Omega$  regions actually might consist of a mixture of two crystallographically unique phases that cannot be distinguished from each other within the  $\Omega$  region by our EDX. We will provide our evidence of this claim below when we discuss the results of x-ray refinements. For each value of y, EDX analysis was done on at least four different areas of the sample and within each are on each region  $(\Phi, \Omega, \text{ or } \Delta)$ . The results are displayed in table 1, table 2, and table 3. The value is the average and the number in the parenthesis covers the spread of all values. It is worth noting that the Ce values produced by our EDX analysis are always observed to be about 90% their actual values based on standards.

In fig. 2(a) we show a PXRD refinement for the y = 0.6 sample. The agreement between theory and experiment is reasonable and the refinement results  $R_p$  and  $R_{wp}$  can be read for each y value from table 4. The refinements required that we include four phases. One of these is the  $\alpha$  Fe phase associated with the  $\Delta$  region. Another is the ThMn<sub>12</sub> type phase of the  $\Phi$  region. To fit the remaining peaks we needed to use two phases. One of the phases has the structure of a Th<sub>2</sub>Ni<sub>17</sub> type which was modeled with Ce replacing Th and Fe replacing Ni. The second of these two phases was a disordered CaCu<sub>5</sub> type phase. The CaCu<sub>5</sub> type phase was modeled after the results of Psycharis et al. in [13]. We used the same ocuppancies listed for the neutron results of Table 1 of [13] and we replaced the Y from [13] with Ce for our x-ray refinements. These last two

phases used for refinements are clearly only approximations. None of Co, Ti, or Si were used as atom types, only Fe, and we clearly cannot determine site preferences in this way or if the occupancies in Table 1 of [13] are the best choice for our data. Our PXRD patterns simply cannot give this much detail. However, all attempts at fitting the remaining reflections after the obvious  $\alpha$  Fe and ThMn<sub>12</sub> phases had already been included failed. The best single phase attempt at that point was a disordered TbCu<sub>7</sub> phase, see for example [14], but this three phase model with the TbCu<sub>7</sub> type proved inadequate. In fig. 2(b) we show a closeup view of the refinement for full disclosure. Some of the intensities are not well fit. However all peak positions are well described. All of the peaks with poorly described intensities belong to either the CaCu<sub>5</sub> type phase or the Th<sub>2</sub>Ni<sub>17</sub> type phase, a fact that indicates our simple model is not quite sufficient. We believe that the  $\Omega$  regions in fig. 1 consist of both the CaCu<sub>5</sub> type phase and the Th<sub>2</sub>Ni<sub>17</sub> type phase. We can say no more about the detailed makeup of the  $\Omega$  regions. Neither the CaCu<sub>5</sub> or Th<sub>2</sub>Ni<sub>17</sub> structure type is required for refinement of the y=0, y=0.2, or y=0.4 data. This is consistent with EDX observations. In fig. 2(c) we display the lattice parameters of the  $ThMn_{12}$  type phase plotted as a function of x. There is a monotonic decrease of both a and c which is expected from atomic radius considerations.

#### 3.2. Magnetic Properties

of The magnetic properties the CeFe<sub>8</sub>Co<sub>3</sub>Ti<sub>1-v</sub>Si<sub>v</sub> ingots were also investigated. Since single phase samples could not be isolated, the magnetic properties will be reported as a function of y and in units that do not require specific knowledge of intrinsic phase properties like density, etc. The same samples used for the PXRD measurements could also be used for magnetization measurements. Each powder was checked to be uniaxial with an easy c axis for the ThMn<sub>12</sub> phase using powder x-ray diffraction on samples aligned in epoxy. Those samples were created in a way previously described [15]. These samples could be used to measure the hard axis field sweeps shown in fig. 3(a). Fits of these curves can return the anisotropy constants and yield  $H_a$ ; such fits are unnecessary here. The curves for the  $y \leq 0.5$ samples are nearly identical with  $H_a$  around 20 kOe, which was about the same result as the CeFe<sub>8</sub>Co<sub>3</sub>Ti sample in [8]. The easy direction

curves are also displayed in fig. 3(a). The curves corresponding to the y = 0.6 sample do not match the rest. The saturation value increases and the signal looks as if it contains contribution from a soft magnetic phase or one with planar anisotropy or both. These results are difficult to interpret due to the phase coexistence already described. The saturation magnetizations were measured on both polycrystalline chunks of material and on the powders used for PXRD and for the hard axis field sweeps. Multiple chunks were analyzed because of irreproducibility at higher y values. The results of all the measurements of  $M_s$  are displayed in fig. 3(b). The likely cause of irreproducibility in the larger y samples is the growth of the Fe-Co alloy phase, which has a huge soft magnetic signal. The same answer is not returned for each chunk because of apparent distribution differences in different chunks. One can, however, see that for  $y \leq 0.4$  that  $M_s$  measurements on various samples of fixed y are very reproducible and it appears that  $M_s$  stays nearly constant in this range and it is not unreasonable to assume that  $M_s$  might behave this way for the complete range of  $0 \le x \le 0.55$ within the CeFe<sub>8</sub>Co<sub>3</sub>Ti<sub>1-x</sub>Si<sub>x</sub> phase, though it is impossible to prove that using the y = 0.5 and y = 0.6 ingots examined in this work.

The Curie temperatures were measured for all of the ingots produced for this study as well. The results are displayed in fig. 4. Thermo-gravitational measurements were performed for the determination of  $T_C$ . Changes in apparent weight, plotted in fig. 4(a), could be used to determine  $T_C$ . Maxima in the first derivative curves tend to give best determinations of  $T_C$  in standards and this analysis is shown in fig. 4(c) and the results for  $T_C$ shown in fig. 4(d).  $T_C$  goes up as the volume of the CeFe<sub>8</sub>Co<sub>3</sub>Ti<sub>1-x</sub>Si<sub>x</sub> phase contracts with increasing x up to x = 0.4, consistent with enhanced hybridization and, thus, enhanced magnetic exchange. We observe a slight decreasing  $T_C$  for x = 0.5 and x = 0.55 samples. The figure displayed in fig. 3(b) is interesting, though not particularly relevant to the study of the CeFe<sub>8</sub>Co<sub>3</sub>Ti<sub>1-x</sub>Si<sub>x</sub> system here. Figure 3(b) is the same type of curve as that displayed in fig. 3(a) but at lower temperatures. The y = 0.6curve displays a kink in the apparent weight that is almost certainly indicitive of  $T_C$  of a phase within the  $\Omega$  region. Unfortunately, because of our inability to isolate the separate compounds of the y = 0.5and y = 0.6 ingots, we cannot determine the specific nature of the phase that caused this feature.

#### 4. Conclusions

We have studied the formation of phases in the nominal system CeFe<sub>8</sub>Co<sub>3</sub>Ti<sub>1-v</sub>Si<sub>v</sub> for  $y \le 0.6$  and found that for  $y \leq 0.4$  arcmelted then 1000 °C annealed and quenched ingots are nearly single phase and correspond to the tetragonal,  $ThMn_{12}$  type phase  $CeFe_8Co_3Ti_{1-x}Si_x$ , where y = x for small values of y. We find, however, for y = 0.5 we start to observe the formation of a new, distinct region in SEM images. At y = 0.6 the observed value for x is only = 0.55 because of the growth of this type of region and also the growth of a region with a structure like  $\alpha$  Fe. For  $x \leq 0.4$  samples the magnetic anisotropy field and saturation magnetizations are all nearly identical while the Curie temperatures increase about 20 °C for increasing y in this range of excellent homogeneity. Above y = 0.4definitive statements about the magnetic properties of the  $CeFe_8Co_3Ti_{1-x}Si_x$  phase become difficult to make due to phase region coexistence and some non-uniform distribution of phase regions in the ingots. We do, however, observe through EDX analysis on multiple areas of y=0.5 and y=0.6 samples that the compositions within these regions is homogeneous.

#### 5. Acknowledgments

The authors of this report wish to thank D. S. Parker for helpful discussions. B.S.C., and B.C.S. acknowledge support from the Critical Materials Institute, an Energy Innovation Hub, funded by the U.S. department of Energy, Office of Energy Efficiency and Renewable Energy, Advanced Manufacturing Office. M.A.M. acknowledges support from the U.S. Department of Energy, Office of Energy Efficiency and Renewable Energy, Vehicle Technologies Office, Propulsion Materials Program. M.A.S. acknowledges support from the U.S. Department of Energy, Office of Science, Basic Energy Sciences, Materials Sciences and Engineering Division

- [1] J. Herbst.  $R_2Fe_{14}B$  materials intrinsic-properties and technological aspects. Rev. Mod. Phys., 63(4):819–898, October 1991.
- [2] J. Florio, R. Rundle, and A. Snow. Compounds of thorium with transition metals - the thorium-manganese system. Acta Crystallographica, 5(4):449–457, 1952.
- [3] F. R. de Boer, Y. Huang, D. B. de Mooij, and K. H. J. Buschow. Magnetic properties of a series of novel ternary intermetallics (RFe<sub>10</sub>V<sub>2</sub>). *Journal of the Less* Common Metals, 135(2):199–204, November 1987.
- [4] R. Verhoef, F. R. de Boer, Z. Zhang, and K. H. J. Buschow. Moment reduction in RFe<sub>12-x</sub>T<sub>x</sub> compounds

- (R=Gd, Y and T=ti, Cr, V, Mo, W). J. Magn. Magn. Mater., 75(3):319–322, December 1988.
- [5] M. Dirken, R. Thiel, and K. H. J. Buschow. Magnetic-anisotropy in ThMn<sub>12</sub>-type compounds studied by Gd-155 Mossbauer-spectroscopy. *Journal of the Less-Common Metals*, 146(1-2):L15–L18, January 1989.
- [6] R. Coehoorn. Electronic-structure and magnetism of transition-metal-stabilized YFe<sub>12-x</sub>M<sub>x</sub> intermetallic compounds. Phys. Rev. B, 41(17):11790–11797, June 1990.
- [7] Department of Energy. CMI annual report. Technical report, Page 5, United States of America, 2016.
- [8] C. Zhou, F. Pinkerton, and J. Herbst. Magnetic properties of CeFe<sub>11-x</sub>Co<sub>x</sub>Ti with ThMn<sub>12</sub> structure. J. Appl. Phys., 115(17):17C716, May 2014.
- Q. Pan, Z. Liu, and Y. Yang Structural and magnetic properties of Ce(Fe, M)<sub>12</sub>N<sub>x</sub> interstitial compounds, M=Ti, V, Cr, and Mo J. Appl. Phys., 76:6728–6730, 1904
- [10] M. Akayama, H. Fujii, K. Yamamoto, and K. Tatami Physical properties of nitrogenated RFe $_{11}$ Ti intermetallic compounds (R = Ce, Pr and Nd) with ThMn $_{12}$  type structure J. Magn. Magn. Mat., 130:99–107, 1994.
- [11] C. Zhou, F. Pinkerton, and J. Herbst. High Curie temperature of Ce-Fe-Si compounds with ThMn<sub>12</sub> structure. Scr. Mater., 95:66–69, January 2015.
- [12] J. Rodriguez-Carvajal. Recent advances in magnetic structure determination by neutron powder diffraction. *Physica B*, 192(12):55 – 69, 1993.
- [13] V. Psycharis, M. Gjoka, C. Christides, and D Niarchos Phase stability, structure and magnetic properties of R<sub>3</sub>(Fe, TM)<sub>29</sub> (R=Gd, Dy, Er, Y and TM = V, Ti) compounds with disordered structures J. Alloy. Compd., 317-318:455-458, 2001.
- [14] C. Zhou, F. Pinkerton, and J. Herbst. Formation of TbCu<sub>7</sub>-type CeFe<sub>10</sub>Zr<sub>0.8</sub> by rapid solidification. *J. Alloy. Compd.*, 569:6–8, August 2013.
- [15] B. S. Conner, M. A. McGuire, K. V. Shanavas, D. S. Parker, and B. C. Sales. Evolution of structural and magnetic properties in  $\text{La}_{\mathbf{x}}\text{Ce}_{2-\mathbf{x}}\text{Co}_{16}\text{Ti}$  for  $0 \leq x \leq 2$ . Journal of Alloys and Compounds, In Press.

Table 1:  $\Phi$  region EDX results

Nominal Comp.	% Fe	% Co	% Ce	% Ti	% Si	Approximate Formula
y = 0	61.7(5)	23.1(4)	6.9(2)	8.1(3)	0.3(2)	$CeFe_8Co_3Ti$
y = 0.2	61.4(2)	23.6(3)	7.1(3)	6.4(4)	1.5(2)	$\mathrm{CeFe_{8}Co_{3}Ti_{0.8}Si_{0.2}}$
y = 0.4	61.3(4)	23.7(3)	7.1(1)	5.1(3)	2.9(2)	$\mathrm{CeFe_{8}Co_{3}Ti_{0.6}Si_{0.4}}$
y = 0.5	61.5(8)	23.4(8)	7.0(2)	4.2(3)	4.0(4)	$\mathrm{CeFe_{8}Co_{3}Ti_{0.5}Si_{0.5}}$
y = 0.6	60.5(5)	23.9(2)	7.0(2)	3.9(2)	4.7(3)	$\mathrm{CeFe_{8}Co_{3}Ti_{0.45}Si_{0.55}}$

Table 2:  $\Omega$  region EDX results

		.0 .			
Nominal Comp.	% Fe	% Co	% Ce	% Ti	% Si
y = 0	_	1	-	-	— ) <i>'</i>
y = 0.2	_	-	_	1	
y = 0.4	_	1	-		<b>)</b> –
y = 0.5	60.5(7)	24.3(9)	8.6(1)	2.9(2)	3.8(2)
y = 0.6	59.1(4)	24.9(4)	8.4(2)	2.7(2)	4.9(4)

Table 3:  $\Delta$  region EDX results

1	abic 5. <u>—</u> .	region LD	r r courto		
Nominal Comp.	% Fe	% Co	% Ce	% Ti	% Si
y = 0	75.1()	18.1()	0.6()	6.1()	0.1()
y = 0.2	77.4()	16.5()	1.1()	4.5()	0.4()
y = 0.4	77.3()	17.7()	0.8()	3.1()	1.0()
y = 0.5	78.2()	18.4()	0.9()	1.6()	0.9()
y = 0.6	77.8()	18.6()	0.8()	1.5()	1.3()

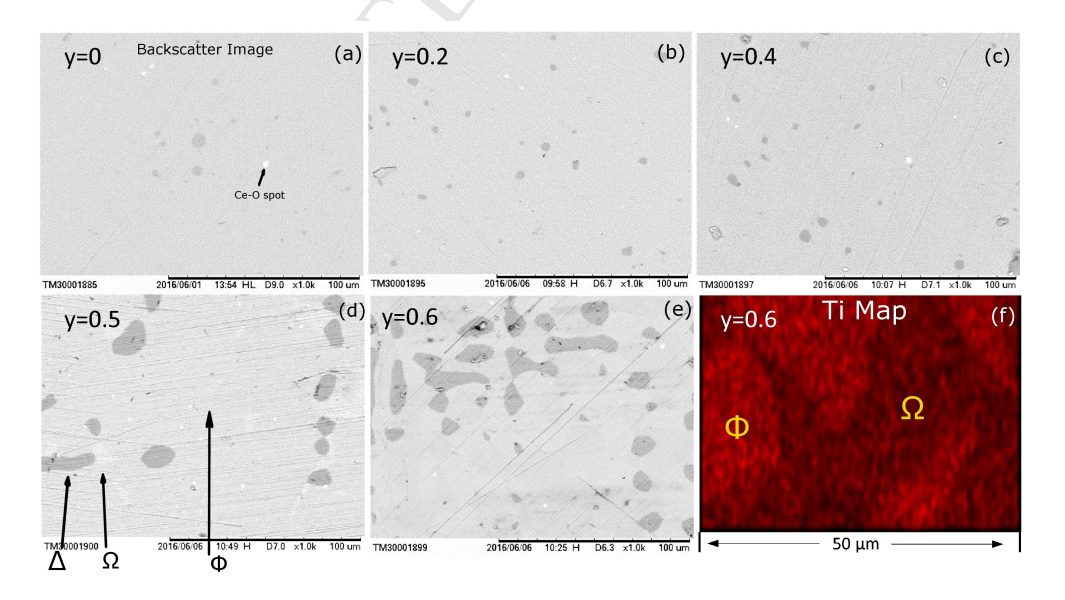


Figure 1: (a-e) Back-scatter SEM images of polished surfaces of CeFe<sub>8</sub>Co<sub>3</sub>Ti<sub>1-y</sub>Si<sub>y</sub> ingots.  $\Phi$ ,  $\Delta$ , and  $\Omega$  type regions are defined in the results section. (f) A false color Ti EDX map to show the distinguishability of the  $\Omega$  and  $\Phi$  regions.

	T III D	D (; (04)
	Lattice Parameters	Proportion (%)
$y = 0.0 (R_p=3.1; R_{wp}=4.3)$		
disordered $CaCu_5$ type	_	0
$ThMn_{12}$ type	a = 8.52729(14); c = 4.75978(10)	96.2
$\mathrm{Th_2Ni_{17}}$ type	-	0
$\alpha$ Fe type	a = 2.88463(58)	3.8
$y = 0.2 (R_p = 2.5; R_{wp} = 4.1)$	5	
disordered $CaCu_5$ type	- /	0
$ThMn_{12}$ type	a = 8.51120(22); c = 4.75651(14)	97.9
$Th_2Ni_{17}$ type	_	0
$\alpha$ Fe type	a = 2.87833(86)	2.1
$y = 0.4 (R_p = 2.3; R_{wp} = 3.4)$	<b>* \ \ \</b>	
disordered $CaCu_5$ type		0
$ThMn_{12}$ type	a = 8.49605(16); c = 4.75369(10)	98.2
$Th_2Ni_{17}$ type	7 -	0
$\alpha$ Fe type	a = 2.87455(50)	1.8
$y = 0.5 (R_p = 2.1; R_{wp} = 2.8)$	⟨ ≻ \ <sup>y</sup>	
disordered CaCu <sub>5</sub> type	a = 4.86394(108); c = 4.18172(130)	4.0
$ThMn_{12}$ type	a = 8.48577(14); c = 4.75285(9)	82.6
$Th_2Ni_{17} type$	a = 8.43980(79); c = 8.35833(134)	5.4
$\alpha$ Fe type	a = 2.87055(16)	8.0
$y = 0.6 (R_p=1.8; R_{wp}=2.5)$		
disordered $CaCu_5$ type	a = 4.86820(20); c = 4.17741(22)	25.0
$ThMn_{12}$ type	a = 8.48009(15); c = 4.75205(10)	47.0
$\mathrm{Th_2Ni_{17}}$ type	a = 8.43336(27); c = 8.35467(46)	15.4
$\alpha$ Fe type	a = 2.87064(10)	12.6

Table 4: Results of powder x-ray diffraction refinements

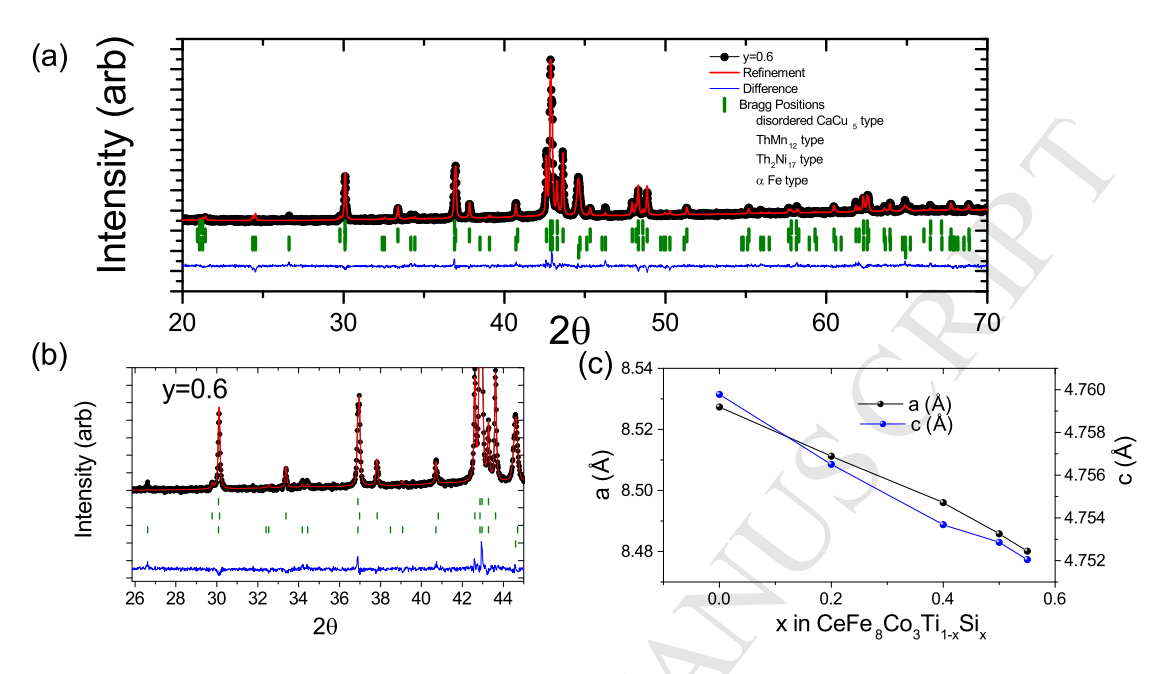


Figure 2: (a) A PXRD pattern and refinement for the y=0.5 sample as defined in the text. (b) A similar figure for the y=0.6 sample with arrows indicating the appearance of two peaks of unknown origin. (c) A plot of the lattice parameters of the ThMn<sub>12</sub> phase with composition CeFe<sub>8</sub>Co<sub>3</sub>Ti<sub>1-x</sub>Si<sub>x</sub>. Note that  $y \neq x$  when y=0.6.

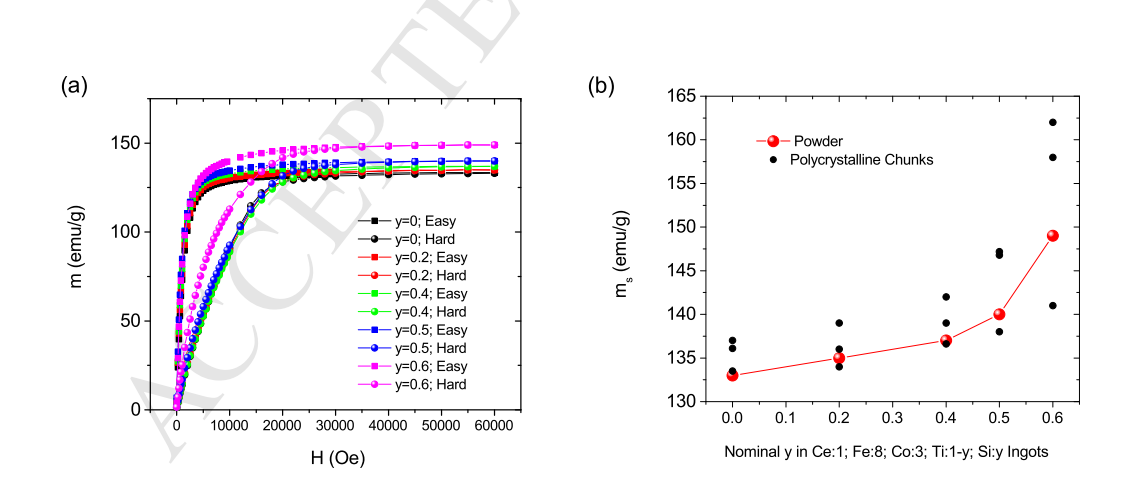


Figure 3: (a) Easy and hard axis field sweeps of field aligned powder samples. These represent multiple phases for y=0.5 and y=0.6. (b) The saturation magnetizations measured on many different samples as a function of y. Here, non-uniform volume distribution of the  $\Delta$  regions in fig. 1 is the likely cause of the large spread in the y=0.6 data.

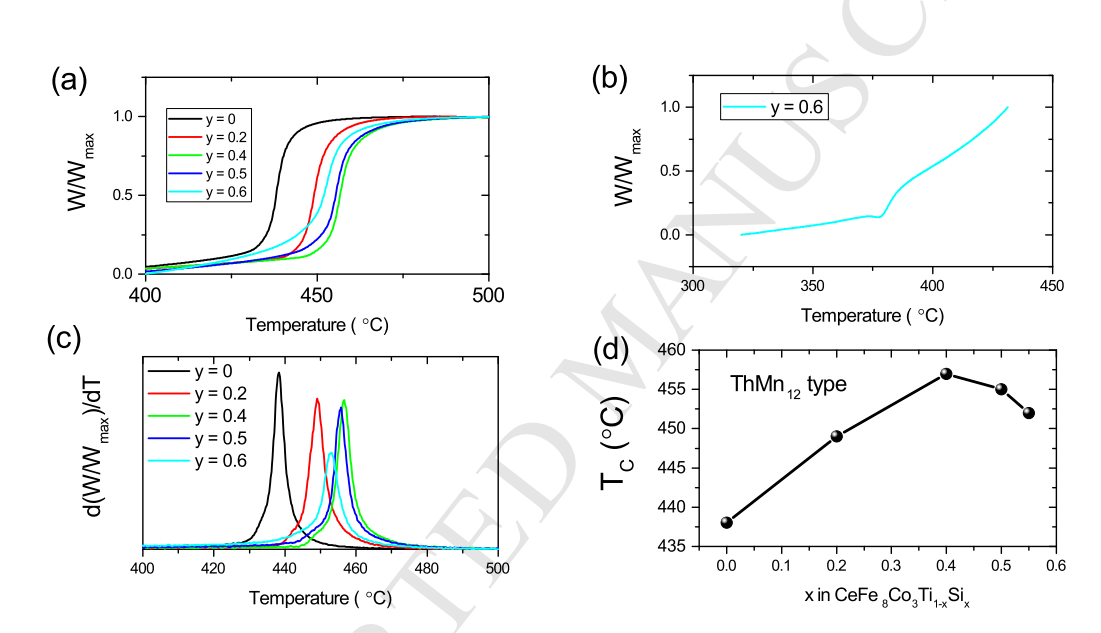


Figure 4: (a) Apparent weight TGA curves in an applied field scaled so that the maximum in the range is 1. (b) A lower temperature version of the same apparent weight curves showing the presumed  $T_C$  near 370°C of a phase within the  $\Omega$  region.. (c) Derivative curves whose maxima determine  $T_C$ . (d)  $T_C$  vs. x for the CeFe<sub>8</sub>Co<sub>3</sub>Ti<sub>1-x</sub>Si<sub>x</sub> type phase.

## Research Highlights:

- CeFe<sub>8</sub>Co<sub>3</sub>Ti<sub>1-x</sub>Si<sub>x</sub> is studied as x is increased from 0 to 0.55.
- For increasing x the samples remain nearly single phase up to x=0.4.
- The saturation magnetization and anisotropy field stay nearly constant.
- The Curie temperature increases for increasing x up to x=0.4 by 20 degrees C.
- A phase with a large Curie temperature emerges alongside larger x samples.